iScience

Article

Decoding aging in the heart via single cell dual omics of non-cardiomyocytes

Graphical abstract

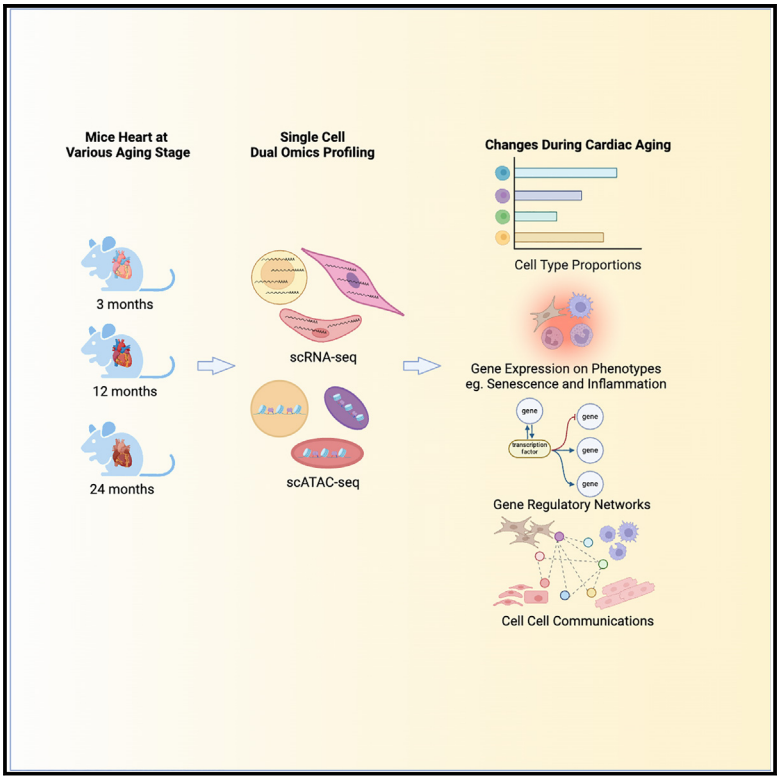

Authors

Yiran Song, Li Wang, Haofei Wang, Hong Ma, Jun Xu, Jiandong Liu, Li Qian

Correspondence

li_qian@med.unc.edu

In brief

Biological sciences; Cell biology; Omics; Transcriptomics

Highlights

- Single cell dual-omics profiling reveals nonmyocyte heterogeneity in heart aging
- Aging non-cardiomyocytes show cell-type-specific transcriptomic and epigenomic shifts
- Senescence-associated secretory phenotype (SASP) elevates in macrophages and fibroblasts
- Fibroblast subcluster with ERBB4 expression shows unique aging impact and cell interactions

Song et al., 2024, iScience 27, 111469
December 20, 2024
https://doi.org/10.1016/j.isci.2024.111469

CellPress

iScience

CellPress
OPEN ACCESS

Article

Decoding aging in the heart via single cell dual omics of non-cardiomyocytes

Yiran Song,[1,2,3,4] Li Wang,[1,2,4] Haofei Wang,[1,2] Hong Ma,[1,2] Jun Xu,[1,2] Jiandong Liu,[1,2] and Li Qian[1,2,3,5,*]
[1]Department of Pathology and Laboratory Medicine, University of North Carolina, Chapel Hill, NC 27599, USA
[2]McAllister Heart Institute, University of North Carolina, Chapel Hill, NC 27599, USA
[3]Department of Biostatistics, University of North Carolina, Chapel Hill, NC 27599, USA
[4]These authors contributed equally
[5]Lead contact
*Correspondence: li_qian@med.unc.edu
https://doi.org/10.1016/j.isci.2024.111469

SUMMARY

To understand heart aging at the single-cell level, we employed single-cell dual omics (scRNA-seq and scATAC-seq) in profiling non-myocytes (non-CMs) from young, middle-aged, and elderly mice. Non-CMs, vital in heart development, physiology, and pathology, are understudied compared to cardiomyocytes. Our analysis revealed aging response heterogeneity and its dynamics over time. Immune cells, notably macrophages and neutrophils, showed significant aging alterations, while endothelial cells displayed moderate changes. We identified distinct aging signatures within the cell type, including differential gene expression, transcription factor activity, and motif variation. Sub-cluster analysis revealed intra-cell type heterogeneity, characterized by diverse aging patterns. The senescence-associated secretory phenotype emerged as a key aging-related phenotype. Moreover, aging significantly influenced cell-cell communication, especially impacting a fibroblast sub-cluster with high expression of ERBB4. This study elucidates the complex cellular and molecular landscape of cardiac aging and offers guidance for potential therapeutic avenues to treat aging-related heart diseases.

INTRODUCTION

Aging stands at the forefront as a critical risk factor for a myriad of cardiovascular diseases (CVDs), including coronary heart disease, hypertension, ischemic disease, and heart failure, with substantial evidence highlighting its profound impact on cardiac pathophysiology and the heightened vulnerability to heart failure it incurs.[1] Particularly, the ventricle of the heart, pivotal in pumping oxygenated blood throughout the body, undergoes significant morphological and molecular alterations during aging, such as hypertrophic growth and increased susceptibility to stress. This underscores the imperative need to delve into the regulatory mechanisms governing cardiac aging to enhance our comprehension of cardiac aging processes and uncover potential therapeutic avenues. The ventricular complexity, arising from a mixture of cell types such as cardiomyocytes and non-cardiomyocytes (non-CMs), including fibroblasts, endothelial cells, and immune cells, demands a detailed examination of the age-related cellular and molecular alterations. While cardiomyocyte aging has been extensively studied, non-CMs, integral to heart development, physiology, and pathology, warrant deeper investigation for their roles in the aging heart. Cellular senescence is one of the most fundamental mechanisms of aging.[2] Senescence-associated secretory phenotype (SASP), a hallmark of cellular senescence and inflammation, contributes to the development of cardiovascular diseases: atherosclerosis, coronary heart disease, and myocardial infarction.[3] It is characterized by the increased secretion of pro-inflammatory cytokines, chemokines, and proteases, emerges as a pivotal player in the progression of age-related cardiac diseases.

Advances in single-cell technologies, such as single-cell RNA sequencing (scRNA-seq) and single-cell Assay for Transposase-Accessible Chromatin using sequencing (scATAC-seq), have revolutionized our understanding of the transcriptional and epigenetic landscapes at an unprecedented level. These methodologies have enabled detailed examinations of the heart cell transcriptome and epigenome across various species and biological processes. For instance, scRNA-seq has shed light on the dynamics of adult zebrafish heart regeneration in non-cardiomyocytes,[4] the transformation of mouse fibroblasts into induced cardiomyocytes,[5] and the mechanisms underlying human cardiac reprogramming.[6] Similarly, scATAC-seq has been instrumental in delineating epigenomic changes and heterogeneity, revealing networks of transcription factors involved in chromatin accessibility shifts during cardiac reprogramming.[7] Moreover, integrated analyses of scATAC-seq and scRNA-seq datasets have facilitated the identification of key active TFs and the global rewiring of *cis*-regulatory interactions, during the direct reprogramming of fibroblasts to induced cardiomyocytes.[7] Single-cell dual omics study[8] has unveiled the transcriptomic and epigenomic diversity in adult murine cardiac non-cardiomyocytes, offering insights that complement traditional

techniques such as immunohistochemistry, real-time qPCR, and *in situ* hybridization.

Herein, we performed single-cell dual-omics to delineate the heterogeneity and functional states of adult mice non-cardiomyocyte (non-CM) at three life stages: young adult (3 months), middle age (12 months), and elderly (24 months By characterizing the regulatory landscapes and functional states of major non-CM cell types, including fibroblasts, endothelial cells, and immune cells, we observed that aging impacts these cells in several distinct ways. Aging leads to shifts in cell composition within tissues, notably with a decrease in the Fib.6, a subcluster of fibroblasts, which contributes to cell cohesion. Transcriptional regulation changes manifest as altered gene expression patterns, where there is an increase in SASP, inflammation, and fibrosis genes. Cell communication is disrupted, evident from reduced overall signaling number and increased SASP, inflammation for intercellular interactions. Additionally, chromatin in non-CMs becomes less accessible with age, leading to decreased accessibility and lower overall gene expression, affecting crucial functions such as cell proliferation and repair. These changes elucidate the complex molecular and cellular dynamics influenced by aging in non-CMs provide new insights into how aging affects non-CMs and offer valuable resources for future follow-up studies and target validation that would be helpful for developing therapeutic strategies targeting age-associated cardiovascular diseases.

RESULTS

Single-cell dual omics profiling of non-CMs during cardiac aging

To elucidate the heterogeneous cellular changes and biological events occurring in non-cardiomyocytes (non-CMs) during aging, we harvested and sorted single live non-CMs from the left ventricle of mouse hearts. These cells were then subjected to both scRNA-seq and scATAC-seq (See Figure 1A). After applying filtering and quality control steps (outlined in Figures S1A and S1E for scRNA-seq; Figures S1B and S1F for scATAC-seq), we successfully obtained biological duplicate samples for each time point. Specifically, this resulted in a total of 24,062 high-quality non-CMs from the scRNA-seq data across three time points (3, 12, and 24 months), with two samples per time point (as shown in Figure S1C). In parallel, we processed 22,309 high-quality single nuclei non-CMs for scATAC-seq analysis, also across three time points with two replicates per time point (as visualized in Figures S1D and S1F). Both UMAP visualizations for scRNA-seq (Figure S1C) and scATAC-seq (Figure S1D) show no evidence of batch effects or the emergence of distinct clusters across time points or samples.

Unsupervised clustering identified 21 distinct cell clusters within the non-CM population, representing the major non-CM cell types such as fibroblasts, endothelial cells, macrophages, smooth muscle cells, and immune cells (neutrophils, T cells, and B cells). Similar clustering results were obtained with CelliD, confirming the identification of 21 distinct cell clusters. As illustrated on the UMAP plot (See Figure 1B), major non-cardiomyocyte cell types include 6 fibroblasts sub-clusters, Fib.1 (IL-6 secreted/inflammation related fibroblast[9]), Fib.2 (activated myofibroblast with *DPP4* marker genes[10]), Fib.3 (activated fibroblast with *CILP*, *MEOX1* marker genes[11]), Fib.4 (basal state of fibroblasts with *ADGRL3* marker genes[12]), Fib.5 (adventitial fibroblast with *C3*[13], *APOE, LNMT, CCL19*[11]), Fib.6 (TGF-beta responsive fibroblast with *ERBB4* marker genes[14]); 7 endothelial sub-clusters, Endo.1 (pro-angiogenic endothelial cell[15]), Endo.2 (endothelial cells activated by vascular endothelial growth factor[16]), Endo.3 (sarcopenic endothelial cells[17]), Endo.4 (high-myofibroblast-like endothelial cells with marker genes *TNNT2*[18]), Endo.5 (stress responsive endothelial cells[19]), Endo.6 (artery endothelial cells[20,21]), Endo.7 (vein and lymphatics endothelial cells[22]); and 4 macrophages sub-clusters, MC.1 (resident macrophages[23]), MC.2 (dendritic cells[24]), MC.3 (proinflammatory macrophages[25]), MC/B-cell (mixed gene markers of macrophages and B-cells) and smooth muscle cells and Neutrophil/T/B cells. The marker gene lists are provided (see Table S1).

Although we did not observe the emergence of any new cell cluster, there are obvious changes in cellular composition across the three time-points. By comparing the proportion of each cell type and their sub-clusters, we observed that fibroblasts (FBs), endothelial cells (ECs), and macrophages (MCs) constitute the major non-CM cell population in the heart (See Figure 1C). For macrophages, the subtype marked by MC.1 dominated the macrophage population, while FBs and ECs exhibit a relatively even distribution of subtypes (See Figure 1C). Additionally, both the number and percentage of macrophages among non-CMs consistently decreased starting from 3 months (See Figures 1E and 1F). Neutrophils showed a marked increase at 12 months, while B cells and T cells remained relatively stable between 3 and 12 months but exhibited a larger increase between 12 and 24 months, highlighting the differential impact of aging on various immune cell types. Using Propeller[26] for differential composition analysis, we identified significant changes in specific sub-clusters (See Figures S3A and S3B), including a consistent decrease in fibroblast sub-cluster Fib.6 (p = 0.027), and an increase in B-cells (p = 0.007). These results indicate the heterogeneous response during aging, across cell types, and within the cell type, as shown in the difference of the sub-clusters.

To explore the epigenetic landscape of non-CMs, we analyzed our scATAC-seq data and performed integrative analysis with scRNA-seq. To annotate cellular identities, we integrated scRNA-seq and scATAC-seq data by first estimating gene transcriptional activity using ATAC-seq counts. We then performed canonical correlation analysis combining these scores with scRNA-seq expression data from highly variable genes. After identifying anchors between datasets, we transferred scRNA-seq annotations to scATAC-seq cells, generating a matrix of predictions and confidence scores for each cell (See Figure 1D). We identified 21 cell clusters for the major non-CM cell types, based on consistent gene activity scores for canonical markers of chromatin accessibility in each cell population with the expression levels in scRNA-seq. Our integrative analysis of scRNA-seq and scATAC-seq data has begun to elucidate the transcriptional and epigenetic landscape in non-CM cells, setting the stage for further investigation into age-related changes in these cell types.

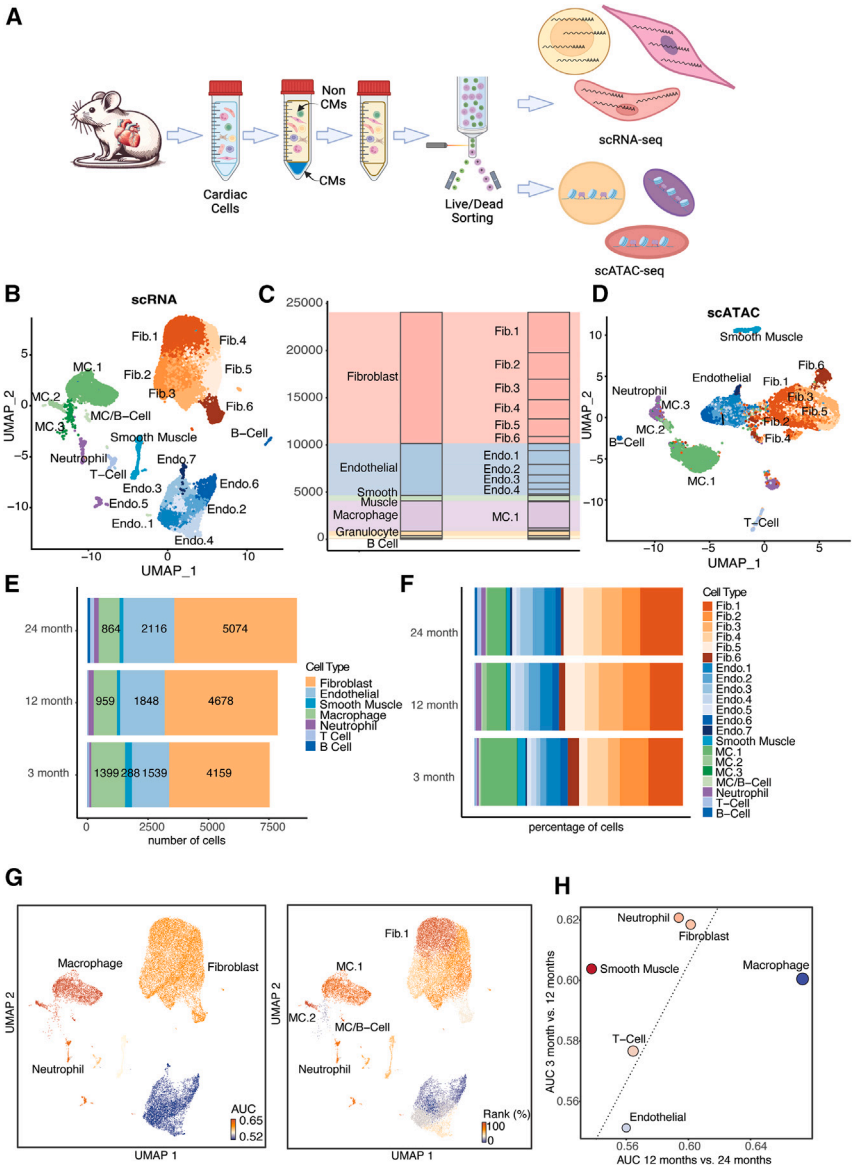

Figure 1. Integrated single-cell transcriptomic and epigenomic analysis of non-cardiac (non-CM) cells during aging

(A) Schematic flowchart illustrating the workflow from cardiac cell isolation to live/dead sorting, followed by single-cell RNA sequencing (scRNA-seq) and single-cell ATAC sequencing (scATAC-seq) to assess transcriptomic and epigenomic changes in non-cardiomyocytes.

(B) UMAP (Uniform Manifold Approximation and Projection) visualization of the 24,062 non-cardiomyocytes identified across six adult mouse hearts. Cells were subclustered into 21 distinct non-CM subtypes, including fibroblasts, endothelial cells, macrophages, neutrophils, and others, shown here with different colors.

(C) River plot shows the total number of major cell types and their respective subtypes.

(D) UMAP visualization of 22,309 non-CM cells captured via scATAC-seq, showing cell types based on chromatin accessibility, highlighting the distribution of major cell populations.

(E) Bar plot showing the number of cells in each main cell type (e.g., fibroblast, endothelial, macrophage, and so forth) across three aging time points (3 months, 12 months, and 24 months).

(F) Bar plot representing the proportion of sub-cell types at each time point, visualizing how the distribution of subtypes changes over time during aging.

(G) UMAP plot shows the score of aging effect in main and sub-cell types of the mouse non-CM cells by Augur. Left panel is colored by the AUC score, which represents the degree to which each cell type is impacted by aging. Darker orange colors indicate higher AUC values, meaning a stronger response to aging, while lighter colors represent lower AUC values, suggesting a weaker aging effect. Macrophages and fibroblasts show higher AUC scores, indicating that these cell types are more impacted by the aging process. Right panel is colored by rank percentages based on the cell-type-specific AUC scores. The rank determines how each cell ranks in terms of its responsiveness to aging, with darker shades indicating higher rank percentages (closer to 100%). The fibroblast sub-cluster Fib.1 and macrophage sub-cluster MC.1 rank higher, suggesting that within these populations, specific cells are more responsive to aging.

(H) Scatterplot comparing AUC scores for each cell type between early aging (3 vs. 12 months) and late aging (12 vs. 24 months). The ΔAUC score shows which cell types exhibit more pronounced transcriptional responses during different stages of aging.

Cell type specific dynamics of non-CMs during cardiac aging

To quantify the impact of aging at the molecular level, we employed the Augur algorithm, which allows us to determine cell type-specific responsiveness to aging.[27] Among the four non-myocyte populations, macrophage's transcriptome showed the highest responsiveness to aging as evident by the highest Area Under Curve (AUC) scores (See Figure 1G). On the other side, endothelial cells' transcriptome showed a relatively minimal change in response to aging. Applying augur on the sub-cluster level, we discovered that not only the macrophage sub-clusters (MC.1 and MC.2) exhibited the most significant transcriptional alterations associated with aging, but also a fibroblast sub-cluster (Fib.1) behaved similarly (See Figure 1G). To investigate the dynamics of cell type-specific responsiveness at different stages of aging, we performed a permutation-based test using Augur (See Figure 1H). Our objective was to determine whether the rate and magnitude of transcriptional changes differ between early (3–12 months) and late (12–24 months) stages of aging for each cell type. We hypothesized that certain cell types might exhibit accelerated transcriptional changes at specific aging phases. In this analysis, we calculated the AUC scores for each cell type by comparing cells from the different age groups. We then permuted the age labels within each cell type 1,000 times to generate a null distribution of AUC differences (ΔAUCs). By comparing the observed

ΔAUCs to this null distribution, we assessed the differences in responsiveness between aging stages for each cell type. Our results indicated that macrophage transcriptomes are more sensitive to aging at the later stages (12–24 months), showing greater transcriptional changes in older mice. In opposite, smooth muscle and neutrophil showed a more drastic change in transcriptome at earlier stages (3–12 months). Interestingly, although the fibroblast's transcriptome showed high responsiveness to aging (See Figure 1G), the rate of transcriptional change remained relatively consistent between the early and late stages. To further explore the impact of parameter tuning on these findings (See Figure S6A) and to compare early and late stages of aging with the entire aging process (3–24 months) (See Figure S6B), we adjusted Augur's parameters. While this led to slight changes in AUC scores, the overall rank of the cell types remained consistent. In summary, our data indicate that the dynamics of the aging-related transcriptome is not a uniform process across cell types. Different cell types in the heart respond to aging at varying degrees and rates, highlighting the complexity of the aging process at the cellular level.

Both cellular senescence and chronic inflammation are recognized hallmarks of aging.[28] Although many studies have examined the cellular senescence and inflammation in the heart, the expression of the aging hallmarks in the non-CM cells and their sub-cell types as well as their aging associated alternations remain largely uncharacterized. Thus, we sought to identify gene signatures linked to key aging cellular features or processes. To this end, we performed AUCell analysis, which calculates the Area Under the recovery Curve, integrating the expression ranks across all genes in a regulon, to score the activity of each regulon in each cell.[29] Our analysis revealed an enrichment in cellular senescence markers, particularly the SASP panel genes. The SASP scores displayed bimodal distributions (See Figure 2A) across all examined time points, with notable elevations in FBs, MCs, and neutrophils, while the ECs have relatively low expression (See Figure 2B). The SASP phenotype showed a significant increase from 3 months to 12 months while remaining at a similar level during the later stage (See Figure 2C). Fibroblast sub-clusters exhibited different trends in their SASP phenotype (See Figure 2D). The Fib.6 sub-cluster demonstrated a significant increase in aging later stage. In contrast, Fib.1 showed a significant increase earlier on. Moreover, we found upregulated gene expressions associated with cardiac fibrosis (See Figures 2E and S2A), heart failure (See Figures 2F and S2B), and inflammation (See Figures 2G and S2C) using the same method as described above. Almost all fibroblast sub-clusters (except Fib.5) (See Figure S2A) showed increases in cardiac fibrosis at least at one time point. For heart failure, only Fib.6 did not exhibit significant increases compared with other fibroblast clusters. The inflammation score was upregulated in most cells, including neutrophils, which displayed a marked increase in the early stages of aging. Interestingly, most endothelial subclusters demonstrated elevated inflammation scores during the early stage (3–12 months) but showed stability in later stages (12–24 months). These results indicate distinct temporal and subtype-specific pro-senescence, pro-fibrotic, and pro-inflammatory signatures in aging non-CMs.

Altered gene expression and cellular communications of non-CMs during cardiac aging

Next, we explored the differential expressed genes (DEGs) in each cell type and their uniquely enriched GO terms (See Figures 3A, 3B, S3C, and S3D). To identify distinct aging-associated changes while minimizing the impact of common cellular molecular signatures, we performed DEG analysis across three aging time points (3, 12, and 24 months). A detailed investigation of cell-type-specific gene expression profiles in endothelial cells, fibroblasts, and macrophages revealed minimal overlap in aging-related DEGs among these cell types (See Figure 3C). Macrophages exhibited the highest number of DEGs, whereas endothelial cells showed fewer DEGs, suggesting fewer changes in endothelial cells during aging, which is consistent with our Augur analysis findings.

To further analyze the gene expression trends over time, we conducted hierarchical clustering of DEGs within each cell type. By using gene expression at 3 months as a reference, we compared the patterns at 12 and 24 months (See Figures 3D and S3E). This clustering revealed distinct expression trajectories, which followed up with GO enrichment analysis for clusters that showed consistent upregulation or downregulation during aging (See Figures 3E and S3F). The GO terms indicate that during cardiac aging, upregulated gene clusters (EC8, FB7, MC8) were predominantly enriched in immune-related functions, whereas downregulated gene clusters (EC4, FB3, MC3) were primarily associated with processes such as cell migration and transcriptional regulation. Specifically, the genes that consistently upregulated in aging endothelial cells (EC8), primarily involved in nitric-oxide synthase activity, detoxification, cellular senescence, and monooxygenase activity, suggest an adaptive enhancement of structural integrity, detoxification processes, and defensive capabilities. Conversely, the deregulated genes (EC4) associated with endothelial cell migration, response to vascular endothelial growth factor stimulus, smooth muscle cell differentiation, and angiogenesis imply a potential decline in angiogenic capacity and responsiveness to angiogenic signals in aging endothelial cells.[30] Similarly, macrophages (MC8) showed a notable upregulation in genes involved in actin polymerization, cell morphogenesis, substrate adhesion, and immune responses, implying enhanced structural integrity, mobility, and immune defense, likely as a compensatory response to the aging-associated decline in cellular function and increased risk of infection. Conversely, the downregulation of genes in MC3 related to T cell activation, immune response coordination, and reactive oxygen species (ROS) metabolism suggests a potential decline in immune function and energy efficiency with aging. In aging fibroblasts, upregulated genes (FB7) were enriched in pathways involving viral process regulation, antigen processing and presentation, intrinsic apoptotic signaling, and immune responses. This suggests a shift toward enhanced immune defense and a higher propensity for apoptosis, potentially as an adaptive response to increased cellular stress during aging. Downregulated genes in fibroblasts (FB3) suggest decreased stress response, and alterations in circadian rhythms.[31,32] Smooth muscle cells (SMC1, SMC2) displayed upregulated oxidative stress-related functions in both early and later stages, indicating an ongoing stress response to the

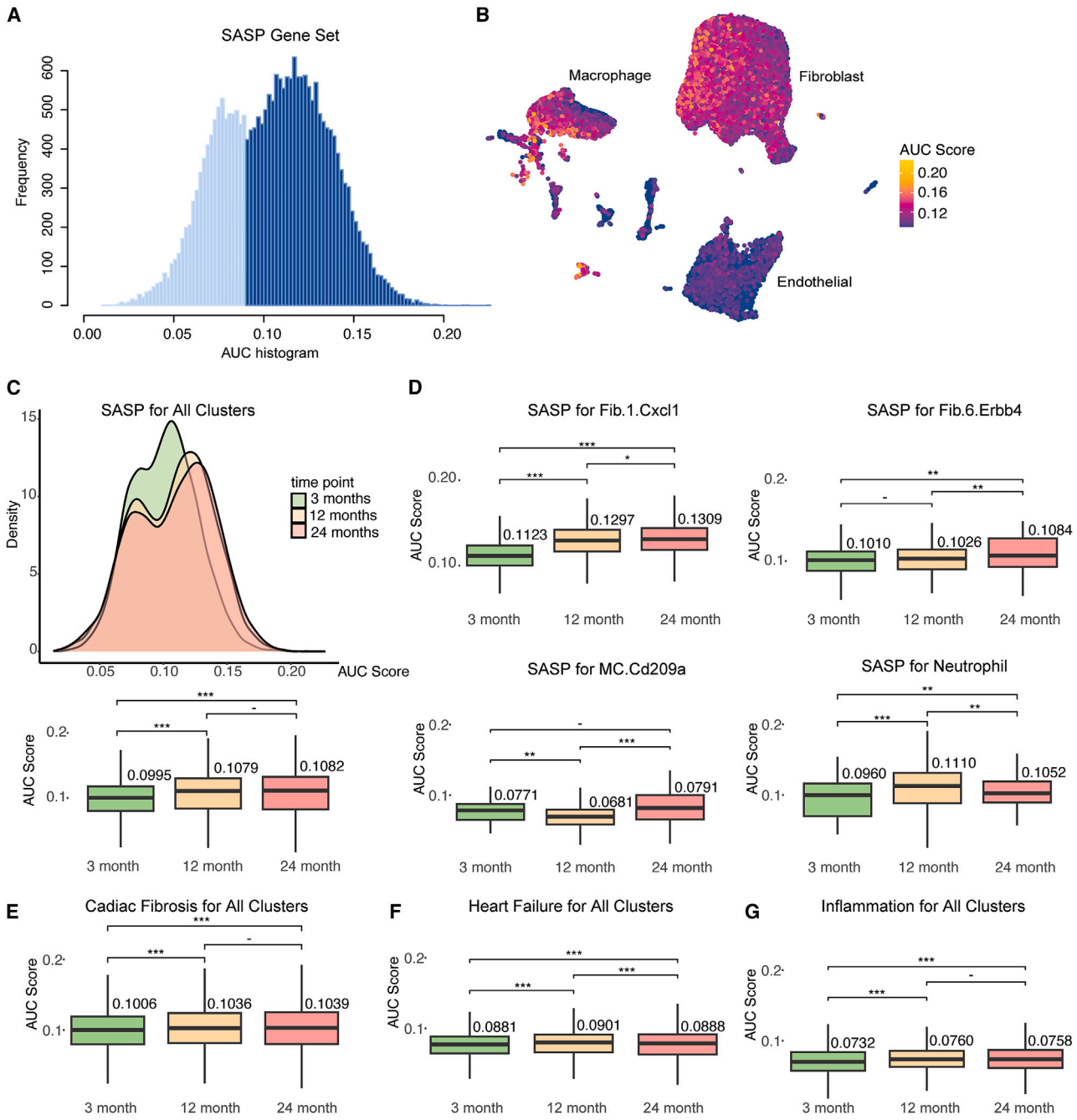

Figure 2. Gene signatures profiling of aging-susceptible of cardiac non-myocyte changes

(A) Bi-modal distribution of senescence-associated secretory phenotype (SASP) gene set score (AUCell) of cardiac non-myocytes.

(B) UMAP plot of the SASP gene set score, showing the highest AUC scores are mainly in Macrophage and Fibroblast cells.

(C) AUC score of the SASP gene set is differentially distributed in three time points. Bar plots show significant changes from 3 months to 12 months (mean ± SEM). Statistical significance is indicated by asterisks (*** $p < 0.001$, ** $p < 0.01$, * $p < 0.05$, based on one-way ANOVA with post-hoc Tukey's test).

(D) AUC score of the SASP gene set has diverse trends in sub cell types, Fib.1.Cxcl1 has continually increased significantly, Fib.6 has a significant increase from 12 to 24 months, while MX.Cd209a decreased and then increased, and neutrophil had a dramatic increase from 3 to 12 months but decreased from 12 to 24 months.

(E) AUC score of the cardiac fibrosis gene set differentially distributed in three time points. Bar plots show significant changes from 3 months to 12 months (mean ± SEM), while no significant changes between 12 and 24 months in all clusters.

(F) AUC score of the heart failure gene set differentially distributes in three time points. Bar plots show a significantly increase from 3 months to 12 months, while a significant decrease between 12 and 24 months in all clusters (mean ± SEM).

(G) AUC score of inflammation gene set differentially distributed in three time points. Bar plots show a significant increase from 3 months to 12 months (mean ± SEM).

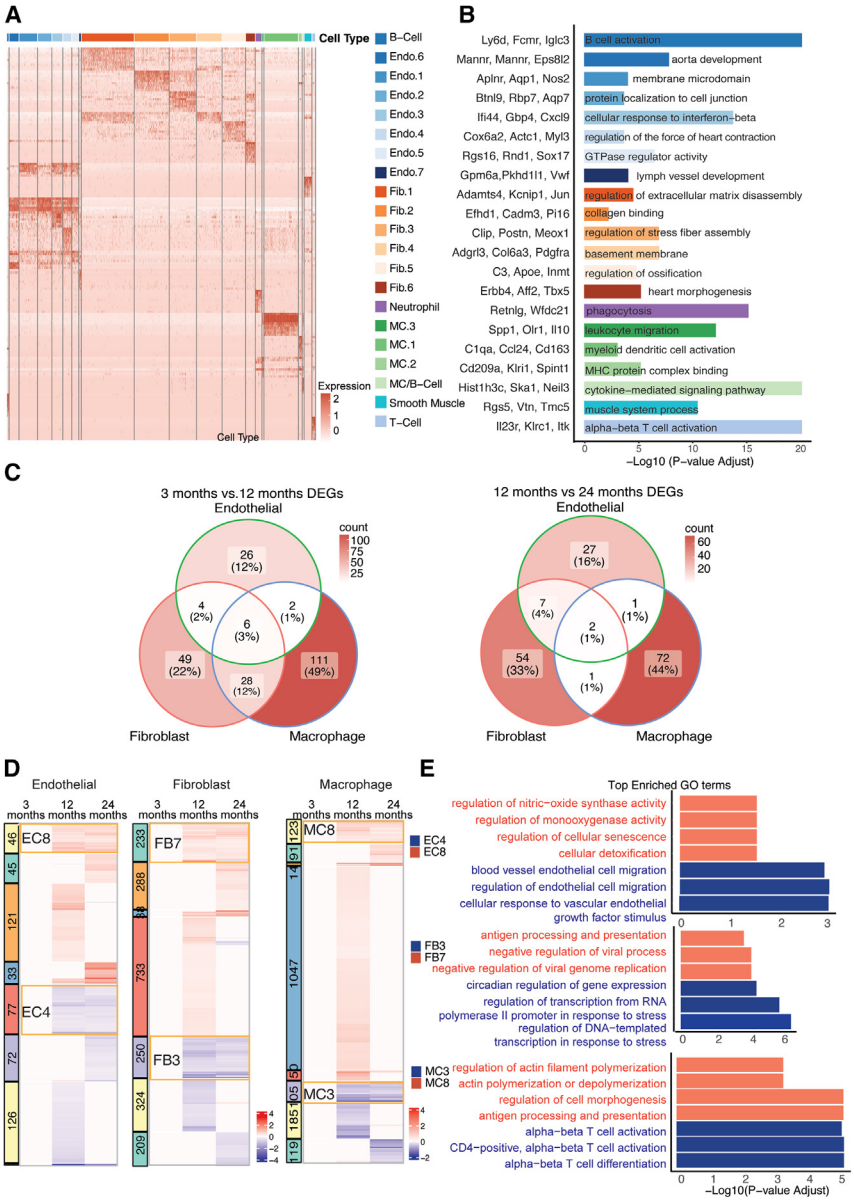

Figure 3. Differentially expressed genes and cluster analysis during aging

(A) Heatmap showing the relative expression levels of representative marker genes across the 21 identified clusters from single-cell RNA-sequencing data.

(B) Unique gene ontology (GO) terms enriched from the differentially expressed genes (DEGs) in the 21 clusters.

(C) Venn diagrams showing the limited overlap of DEGs in three main cell types (endothelial, fibroblast, and macrophage) between the 3 to 12 months and 12 to 24 months comparisons. Number in the Venn plot shows the number and proportion of DEGs for each cell type.

(D) Heatmap of DEGs hierarchically clustered within endothelial, fibroblast, and macrophage cells, using gene expression at 3 months as a reference point for comparison with 12 and 24 months. Numbers along the y axis indicate cluster identifiers, with corresponding DEG numbers on the side of each heatmap. Clusters that show constant changes in expression patterns over time are highlighted.

(E) Top enriched GO terms for clusters that show consistent upregulation (EC8, FB7, MC8 in red) or downregulation (EC4, FB3, MC3 in blue) across aging time points. GO terms related to processes such as nitric oxide synthase activity, endothelial cell migration, cellular detoxification, and antigen processing are featured for specific clusters. The bar plots indicate the degree of enrichment (−log10(*p*-value Adjust)) for these GO terms.

characteristic of advanced aging. These shifts in gene expression could reflect cells' adaptive strategies to aging challenges but may also contribute to the overall decline in cardiovascular health and tissue function observed in older mice.

Aging is also recognized to influence the intercellular communication.[33] We conducted CellChat analysis to analyze the changes of cell-cell communication, focusing on those attributable to aging. As age progressed, we observed a notable decrease in both the intensity and frequency of cellular interactions (See Figure 4A). While there is an increase in communications of macrophage and neutrophils with other cell types from 3 to 12 months of age (See Figure 4B), the transition from mid-age (12 months) to elder age (24 months) showed a decrease in the frequency of cellular interactions, with the exception of T-cells and smooth muscle cells, which exhibited increased communications (See Figure 4B). In the context of overall cellular interactions, we found specific sub-cluster changes. The Endo.7 sub-cluster, for instance, demonstrated augmented interaction strength in receiving signals from fibroblasts during the early aging stage (See Figure 4B). This shift in intensity and frequency of cellular communications suggests a role of endothelial cells in vascular regulation and barrier function, and the influence of fibroblast signaling in extracellular

accumulation of cellular damage (See Figures S3E and S3F). In the early aging stages (3–12 months), there is a pronounced upregulation of genes related to protein folding, stabilization, and response to oxidative stress, suggesting an enhanced ability to manage protein misfolding and oxidative damage. At the same time, genes (SMC3) involved in heat response and cellular heat acclimation are downregulated, potentially reflecting reduced resilience to thermal stress. In the later stages of aging, the downregulation of genes (SMC4) related to cardiac muscle contraction and actin filament-based movement signals a gradual decline in contractile function and structural integrity. However, the upregulation of genes tied to stress responses, along with antigen processing and presentation, points to an adaptive increase in defense mechanisms, likely compensating for ongoing cellular damage and the diminished functionality

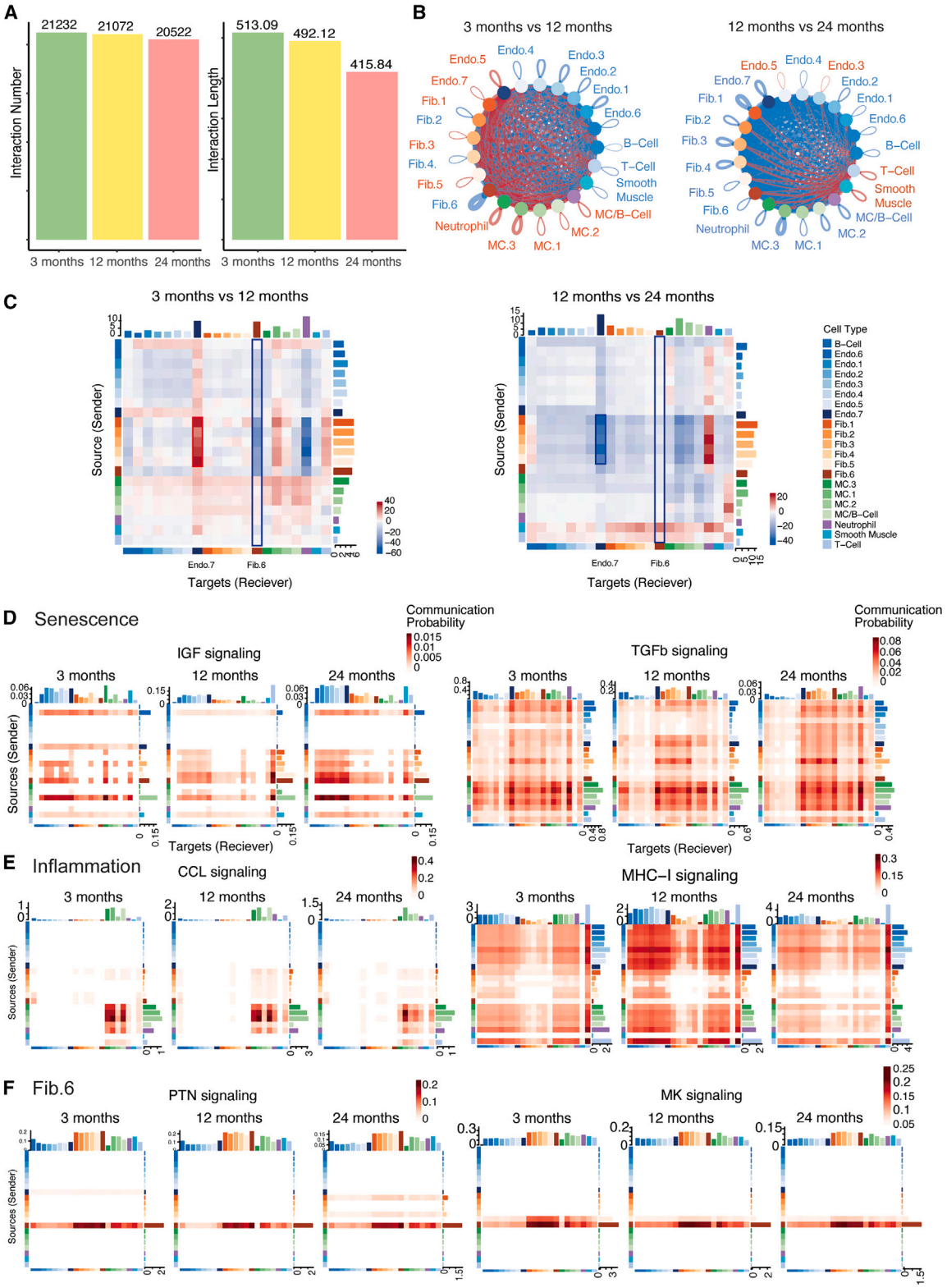

Figure 4. Cell-cell communication during aging

(A) Bar plots represent the changes in both the total number of cell interactions (left) and the overall interaction strength (right) across different time points (3, 12, and 24 months). Both metrics show a general decline during aging.

(legend continued on next page)

matrix production and tissue repair, become increasingly intertwined in the aging heart.[32,34] The Fib.6 sub-cluster (See Figure 4C), however, showed a distinct intercellular communication profile. Initially, it had suppressed interactions, followed by a maintenance of interaction numbers but with reduced strength, signifying a profound impact of aging on its functionality. Moreover, our analysis suggests the prominence of senescence (e.g., *IGF, TGFb*) (See Figure 4D) and inflammation (e.g., *CCL, MHC-I*) pathways (See Figure 4E), with an upsurge during aging. The unique pathway activation in the Fib.6 sub-cluster, involving *MK, PTN, VCAM,* and *ICAM*, (See Figure 4F), highlights its distinct functional contributions amidst aging.

Single cell regulatory network of non-CMs during cardiac aging

To unravel transcription mediators that might regulate non-CM aging, we deployed the Single-Cell Regulatory Network Inference and Clustering (SCENIC) analysis to infer core transcription factors (TFs) functioning in the non-CM cell types. Based on the activity of the regulons, we observed that cells of the same type were re-clustered together, indicating shared TFs and activity, yet distinct activities within the sub-clusters. (See Figure 5A). We can find the clustering of main cell types such as endothelial, immune cells (Macrophages, Neutrophils, T/B cells), and fibroblasts, aligning with our initial clustering findings in spite of the different clustering approaches.

We next sought to determine change in the regulatory network. We, therefore, performed linear mixed models (LMMs), a method that facilitates the identification of TFs with significant shifts in average activity during the aging process, both for overall (See Figures 5B, S4A–S4C, and S5A) and certain cell types (See Figures 5C and 5D; Figure S5B) followed by the GO enrichment. The activity is calculated based on the expression of each TF's target genes in individual cells. For the overall trend, TFs involved in rhythmic and circadian regulation, *HLF, TEF, and DBP*, demonstrated a marked decrease in activity from early adulthood (3 months) to midlife (12 months), followed by a slight increase in later stages (See Figure S4A). Conversely, TFs implicated in immune response regulation, *IRF7, IRF9, and STAT1*, displayed a consistent increase in activity through aging (See Figure S4B; Figures 5B and 5C). A close examination of specific cell types revealed that the FBs exhibited an increase in immune-related TF activity, while the activities of the catabolism and transcription-related TFs, such as *ATF4* and *YY1*, decreased over time with age (See Figure 5C). A similar trend was observed for endothelial cells (See Figure 5D). Macrophages, however, did not exhibit significant changes in TF activity as assessed by LMMs. As an alternative approach, we employed a linear model to identify the top differentially regulated TFs and their associated GO terms (See Figure S5B). The enriched TFs were similar to FBs and ECs, including upregulated *IRF7, STAT1, STAT2,* and downregulated *BACH1, DBP, and JUND*. In sum, fibroblasts have the most differentially changed TFs detected. Macrophages surprisingly do not have many significantly changed regulons, which implies it may not employ new TF regulatory networks during aging and deserve further exploration.

Potential regulators invovled in cardiac aging

We then explored the scATAC-seq dataset to pinpoint regions of differential chromatin accessibility (DAC) and performed motif enrichment on these DACs. These are locations in the genome where the accessibility of the chromatin structure varies, which can influence gene expression (See Figure 6A). Our analysis revealed a lack of peaks that are commonly accessible across three primary cell types. Interestingly, endothelial cells (ECs) showed the least variation in these differentially accessible peaks. This suggests a relatively stable chromatin landscape in ECs during the aging process (See Figure 6B). This observation is further supported by motif analysis; our motif analysis identified a consistent set of transcription factor binding motifs in ECs across the time points, indicating a stable regulatory landscape. In contrast, FBs and macrophages displayed a greater diversity of motif accessibility, suggesting a more dynamic regulatory response to aging. This observation highlights the distinct regulatory patterns across cell types during aging, with ECs maintaining a relatively stable regulatory architecture compared to the more flexible responses observed in FBs and macrophages (See Figure 6D).

Moreover, our scATAC-seq data provided direct evidence for the chromatin open regions and binding motifs, supporting our findings of consensus sequence identification from scRNA-seq. We observed age-related decreases in accessibility for motifs such as *YY1*[35] and *ATF4*,[36] which play roles in cellular catabolism and transcription regulation (See Figures 6C and 6D). In contrast, the motifs for *IRF7* and *STAT1*, known for their role

(B) Circle plots visualizing changes in communication patterns between different cell types across aging time points. Line colors indicate the direction of communication changes: red lines represent increased communication at the later time point, while blue lines represent decreased communication. Line thickness reflects the magnitude of interaction changes, with thicker lines indicating more substantial changes. From 3 to 12 months, macrophages (MC) and neutrophils (in red) exhibit increased communication with other cell types, whereas the Fib.6 sub-cluster shows reduced interactions. Between 12 and 24 months, there is a general decline in cell communication, except for T cells, smooth muscle cells, and certain endothelial subtypes, which show increased interactions.
(C) Heatmaps compare the strength of cell-cell communication at different aging stages (3 vs. 12 months and 12 vs. 24 months). The x axis represents target (receiver) cell types, and the y axis represents source (sender) cell types. The color gradient indicates communication strength, with red representing stronger communication in the later time stage, and blue representing weaker communication in the later time stage.
(D) The senescence phenotype is explored through IGF and TGF-β signaling pathways across different time points (3, 12, and 24 months). Both pathways show an increase in cell signaling related to aging and cellular senescence.
(E) Inflammation-related communication is demonstrated through the CCL and MHC-I signaling pathways. Both pathways show an increase in inflammation as the tissue ages.
(F) The specific role of the Fib.6 sub cluster is highlighted in cell communication during aging. PTN and MK signaling pathways both show decreasing during aging, where Fib.6 is the main sender of the signaling, impacting heart function.

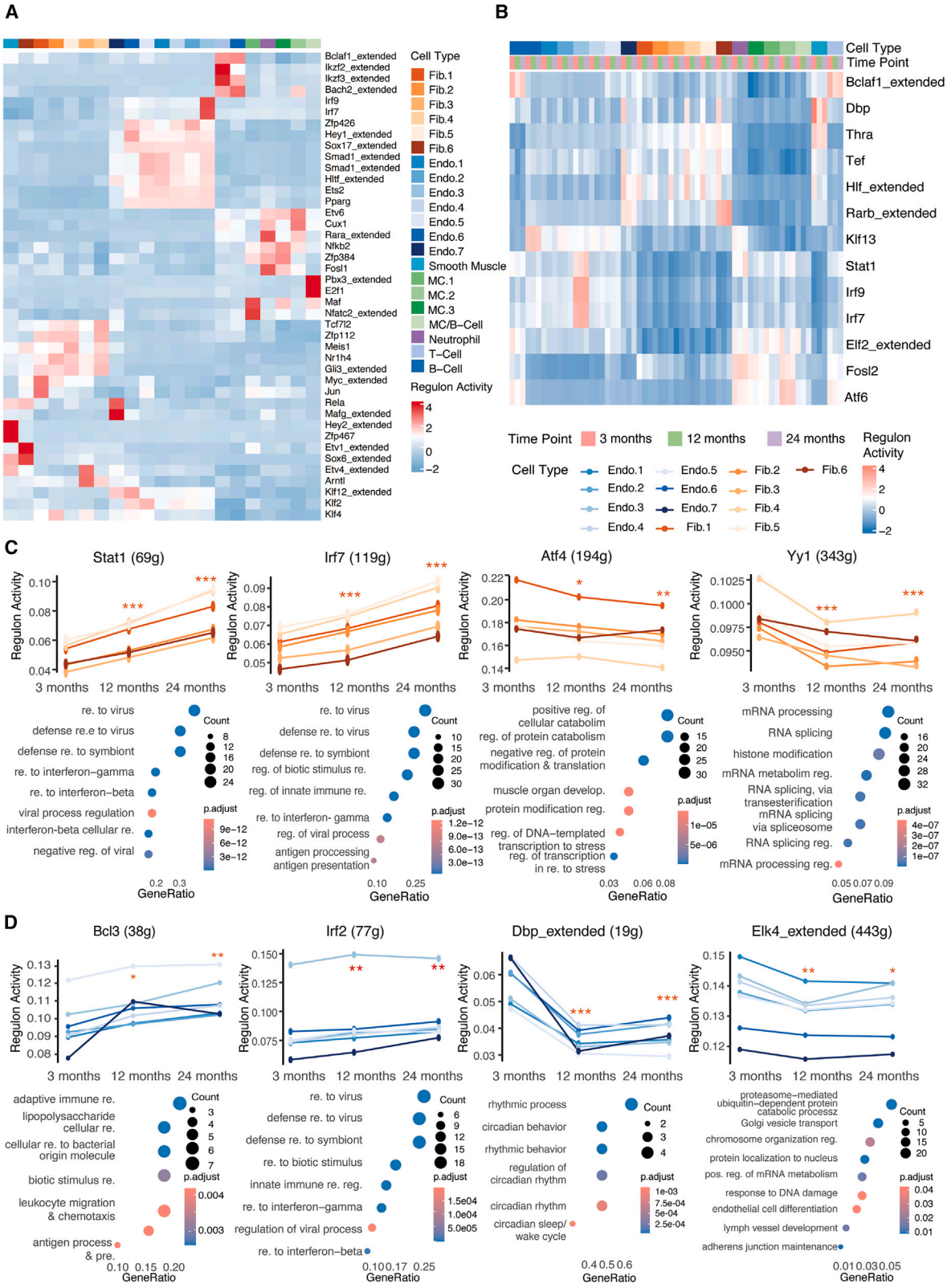

(legend on next page)

in cellular senescence and immune responses, demonstrated increased accessibility, aligning with the increased expression of their corresponding transcription factors in our scRNA-seq (See Figures 5C–5E). Despite observing consistent trends, the complexity of regulatory changes and the mechanisms driving these alterations during aging warrant further investigation. However, it is crucial to acknowledge that the relationship between motif accessibility and transcription factor activity is not entirely correlated, indicating the need for further studies to fully elucidate these dynamics.

DISCUSSION

In this study, we leveraged single-cell dual omics to elucidate the complex landscape of cardiac aging in non-cardiomyocytes (non-CMs). Our comprehensive analysis uncovered cell-type-specific aging signatures and dynamic changes in cell-cell communication among non-CMs in the heart. The heterogeneous yet moderate changes observed with aging emphasize the importance of examining each cell type individually. We demonstrated that fibroblasts and macrophages exhibit the most pronounced aging responses, highlighting the significance of these cell types in cardiac aging processes. In particular, the Fib.6 sub-cluster was notably affected by aging, suggesting it is a potential target for therapies aimed at age-associated cardiovascular diseases. Conversely, endothelial cells exhibited remarkable stability, indicating an inherent resilience to aging processes that warrants further investigation.

One of the striking findings of our study is the role of the SASP in mediating the effects of aging on cardiac non-CMs. This opens up new avenues for therapeutic strategies aimed at mitigating SASP-induced pathology, potentially altering the trajectory of cardiac aging. Additionally, the dynamic transcriptional regulatory networks we uncovered, especially the shifts in activity of transcription factors related to immune responses and circadian regulation, provide deeper insights into the molecular underpinnings of cardiac aging.

In conclusion, our research underscores the importance of non-cardiomyocytes in cardiac aging and lays the groundwork for future investigations into targeted therapeutic strategies for aging-related heart diseases. As we continue to unravel the complexities of cardiac aging, leveraging novel technologies and multidisciplinary approaches will be imperative for developing interventions that can enhance cardiovascular health in the aging population.

Limitations of the study

It is important to acknowledge the limitations of our study. Firstly, we focused exclusively on the ventricles of the heart, without including atrial cells. Given that atrial cells play crucial roles in cardiac function and may exhibit different aging patterns, future studies should include both ventricular and atrial cells to provide a more comprehensive understanding of cardiac aging. Secondly, our study utilized only male mice, and the impact of sex differences on cardiac aging was not addressed. Including both sexes in future research could elucidate potential sex-specific mechanisms in cardiac aging. Additionally, while we employed single-cell dual omics techniques, most analyses were performed separately on scRNA-seq and scATAC-seq data. Integrating these datasets, such as through joint gene network inference, could enhance our findings and offer a more comprehensive view of the regulatory mechanisms at play. Moreover, the translational potential of our findings, while promising, requires further validation in preclinical and clinical settings. By focusing on the responsive cell types and altered communication pathways we identified, future research can explore targeted therapeutic strategies to address aging-related cardiac dysfunction.

RESOURCE AVAILABILITY

Lead contact

Further information and requests for resources and reagents should be directed to and will be fulfilled by the lead contact, Li Qian (li_qian@med.unc.edu).

Materials availability

This study did not generate new unique reagents.

Data and code availability

- Single-cell RNA-seq and ATAC-seq data have been deposited at GEO at GSE277702 and are publicly available as of the date of publication.
- The original code has been deposited at Zenodo and is publicly available at https://doi.org/10.5281/zenodo.14014681 as of the date of publication.
- Any additional information required to reanalyze the data reported in this article is available from the lead contact upon request.

ACKNOWLEDGMENTS

We would like to thank all the members of the Qian and Liu labs for their helpful discussion and valuable input. J.L. is supported by NIH/NHLBI R01HL139976 and R01HL139880, and AHA 20EIA35320128. L.Q. is supported by AHA 20EIA35310348 and NIH/NHLBI R35HL155656. Graphical abstract and Figure 1A are created in BioRender.

Figure 5. Gene regulatory networks during aging by single-cell regulatory network inference and clustering (SCENIC)

(A) Heatmap illustrating the core transcription factors (TFs) with the most active regulon activities across different cell types during aging. Each row represents a TF, while columns indicate the cell type, showcasing the varied activity of regulatory networks in fibroblasts, endothelial cells, macrophages, and other non-cardiomyocytes.

(B) Regulon activity for transcription factors significantly changes during aging, across more than three cell types. The heatmap shows how the activity of TF changes over time in several cell types.

(C) Line plots demonstrating the dynamic changes in fibroblast TF activities over three aging time points (3, 12, and 24 months), based on the linear mixed model analysis. The associated GO enrichment plots show the functional processes these TFs regulate. TFs such as *STAT1*, *IRF7*, and *ATF4* are linked to immune responses and cellular catabolism. Statistical significance is indicated by asterisks (*** $p < 0.001$, ** $p < 0.01$, * $p < 0.05$, based on one-way ANOVA with post-hoc Tukey's test).

(D) Line plots and GO enrichment analyses for endothelial cell-specific TFs with significant changes in activity during aging, derived from the linear mixed model. TFs such as *BCL3*, *IRF2*, and *DBP* demonstrate changes in activities, especially in pathways related to immune regulation and circadian rhythms.

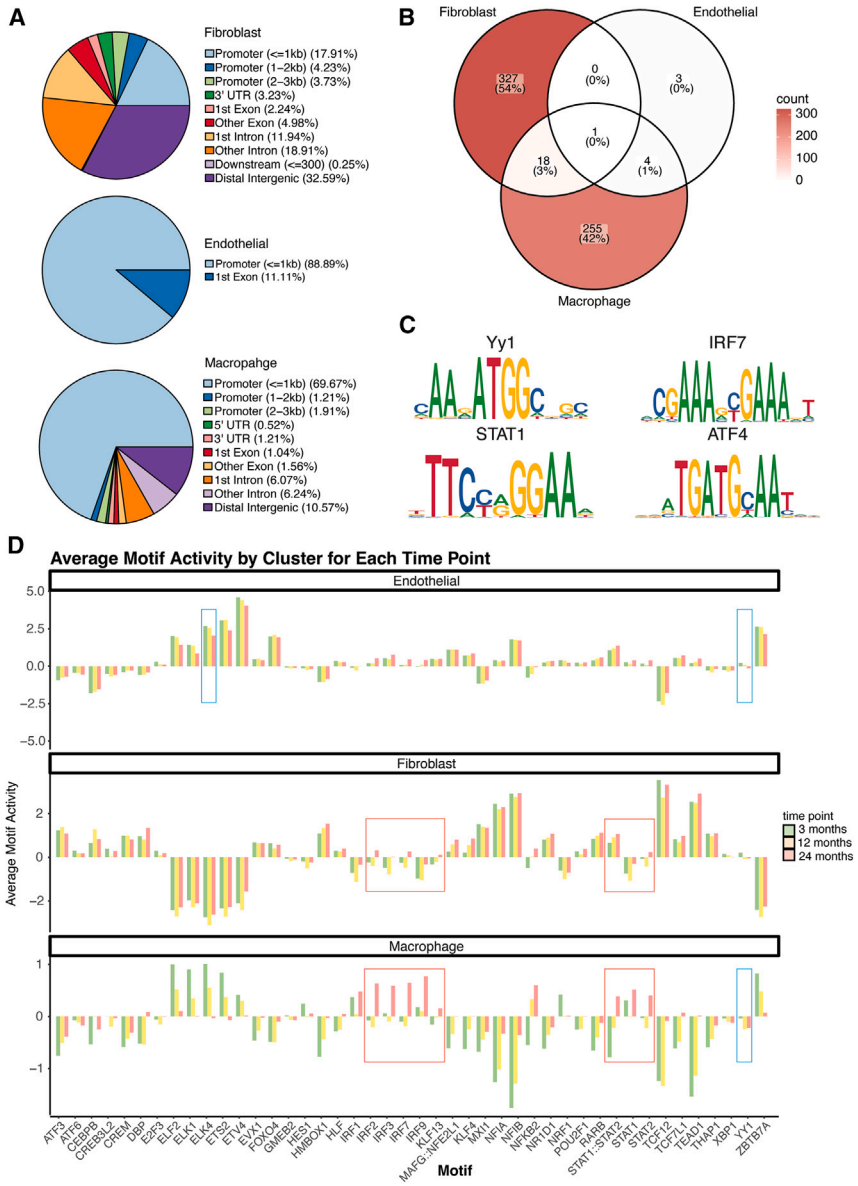

Figure 6. Integrated single-cell ATAC seq epigenomic analysis of non-CM cells during aging

(A) Proportional distribution of gene-near differential accessible peaks (DAPs) across fibroblasts, endothelial cells, and macrophages. Fibroblasts display the greatest diversity in DAPs, covering a broad range of genomic regions such as distal intergenic regions (32.59%) and promoters (17.91% within 1kb), while endothelial cells show more restricted accessibility, primarily focused on promoter regions (88.89%).

(B) Venn diagram illustrates the overlap of DAPs between fibroblasts, endothelial cells, and macrophages. The results demonstrate limited common peaks among the cell types, with fibroblasts and macrophages sharing a small subset of accessible regions, highlighting the distinct epigenetic landscapes in these non-CMs during aging.

(C) Enriched transcription factor binding motifs identified through motif analysis of DAPs, including *YY1, IRF7, STAT1*, and *ATF4*, are consistent with transcription factors (TFs) known to regulate aging-related processes in non-CM cells. These motifs are associated with immune response, cellular stress, and transcription regulation.

(D) Bar plots showing the average motif activity across fibroblasts, endothelial cells, and macrophages at three aging stages (3, 12, and 24 months). Highlighted motifs (e.g., IRF and STAT families) exhibit consistent trends in activity, corresponding to changes observed in transcription factor activity, as indicated by red and blue boxes marking clusters with pronounced activity changes over time.

AUTHOR CONTRIBUTIONS

L.W. and L.Q. designed the study. L.W. and X.J performed experiments. Y.S. analyzed data, interpreted results of experiments, and prepared figures. Y.S. drafted the article. Y.S., H.W., J.L., and L.Q. edited and revised article. J.L. and L.Q. supervised the work and approved final version of article.

DECLARATION OF INTERESTS

The authors declare no competing interests.

DECLARATION OF GENERATIVE AI AND AI-ASSISTED TECHNOLOGIES

During the preparation of this work, the authors used ChatGPT in order to check the grammar. After using this tool or service, the authors reviewed and edited the content as needed and take full responsibility for the content of the publication.

STAR★METHODS

Detailed methods are provided in the online version of this paper and include the following:

- KEY RESOURCES TABLE
- EXPERIMENTAL MODEL AND STUDY PARTICIPANT DETAILS
  - Mouse model
  - Heart collection and nonmyocytes isolation
  - Single-cell transcriptome library preparation and sequencing
  - Single-cell ATAC library preparation and sequencing
- METHOD DETAILS
  - Single-cell RNA-seq data analysis
  - Quality control and preprocessing

- Dimensionality reduction and clustering
- Differentially expressed gene (DEG) analysis
- Gene ontology (GO) over-representation analysis
- Cell type annotation and validation
- Identification of cell types affected by aging perturbations
- Gene set enrichment and pathway analysis
- Hierarchical clustering analysis
- Cell–cell communication analysis
- Transcriptional regulatory network analysis
- Single-cell ATAC-seq data analysis
- Quality control and preprocessing
- Dimensionality reduction and clustering
- Cell type annotation via label transfer
- Differential accessibility analysis
- Motif enrichment and variability analysis

- QUANTIFICATION AND STATISTICAL ANALYSIS
  - Statistical analysis

SUPPLEMENTAL INFORMATION

Supplemental information can be found online at https://doi.org/10.1016/j.isci.2024.111469.

Received: June 11, 2024
Revised: September 30, 2024
Accepted: November 21, 2024
Published: November 28, 2024

REFERENCES

1. Donato, A.J., Machin, D.R., and Lesniewski, L.A. (2018). Mechanisms of Dysfunction in the Aging Vasculature and Role in Age-Related Disease. Circ. Res. *123*, 825–848. https://doi.org/10.1161/CIRCRESAHA.118.312563.
2. Saul, D., Kosinsky, R.L., Atkinson, E.J., Doolittle, M.L., Zhang, X., LeBrasseur, N.K., Pignolo, R.J., Robbins, P.D., Niedernhofer, L.J., Ikeno, Y., et al. (2022). A new gene set identifies senescent cells and predicts senescence-associated pathways across tissues. Nat. Commun. *13*, 4827. https://doi.org/10.1038/s41467-022-32552-1.
3. Khavinson, V., Linkova, N., Dyatlova, A., Kantemirova, R., and Kozlov, K. (2022). Senescence-Associated Secretory Phenotype of Cardiovascular System Cells and Inflammaging: Perspectives of Peptide Regulation. Cells *12*, 106. https://doi.org/10.3390/cells12010106.
4. Ma, H., Liu, Z., Yang, Y., Feng, D., Dong, Y., Garbutt, T.A., Hu, Z., Wang, L., Luan, C., Cooper, C.D., et al. (2021). Functional coordination of non-myocytes plays a key role in adult zebrafish heart regeneration. EMBO Rep. *22*, e52901. https://doi.org/10.15252/embr.202152901.
5. Liu, Z., Wang, L., Welch, J.D., Ma, H., Zhou, Y., Vaseghi, H.R., Yu, S., Wall, J.B., Alimohamadi, S., Zheng, M., et al. (2017). Single-cell transcriptomics reconstructs fate conversion from fibroblast to cardiomyocyte. Nature *551*, 100–104. https://doi.org/10.1038/nature24454.
6. Zhou, Y., Liu, Z., Welch, J.D., Gao, X., Wang, L., Garbutt, T., Keepers, B., Ma, H., Prins, J.F., Shen, W., et al. (2019). Single-Cell Transcriptomic Analyses of Cell Fate Transitions during Human Cardiac Reprogramming. Cell Stem Cell *25*, 149–164.e9. https://doi.org/10.1016/j.stem.2019.05.020.
7. Wang, H., Yang, Y., Qian, Y., Liu, J., and Qian, L. (2022). Delineating chromatin accessibility re-patterning at single cell level during early stage of direct cardiac reprogramming. J. Mol. Cell. Cardiol. *162*, 62–71. https://doi.org/10.1016/j.yjmcc.2021.09.002.
8. Wang, L., Yang, Y., Ma, H., Xie, Y., Xu, J., Near, D., Wang, H., Garbutt, T., Li, Y., Liu, J., and Qian, L. (2022). Single-cell dual-omics reveals the transcriptomic and epigenomic diversity of cardiac non-myocytes. Cardiovasc. Res. *118*, 1548–1563. https://doi.org/10.1093/cvr/cvab134.
9. Nguyen, H.N., Noss, E.H., Mizoguchi, F., Huppertz, C., Wei, K.S., Watts, G.F.M., and Brenner, M.B. (2017). Autocrine Loop Involving IL-6 Family Member LIF, LIF Receptor, and STAT4 Drives Sustained Fibroblast Production of Inflammatory Mediators. Immunity *46*, 220–232. https://doi.org/10.1016/j.immuni.2017.01.004.
10. Soare, A., Györfi, H.A., Matei, A.E., Dees, C., Rauber, S., Wohlfahrt, T., Chen, C.-W., Ludolph, I., Horch, R.E., Bäuerle, T., et al. (2020). Dipeptidyl-peptidase 4 as a Marker of Activated Fibroblasts and a Potential Target for the Treatment of Fibrosis in Systemic Sclerosis. Arthritis Rheumatol. *72*, 137–149. https://doi.org/10.1002/art.41058.
11. Patrick, R., Janbandhu, V., Tallapragada, V., Tan, S.S.M., McKinna, E.E., Contreras, O., Ghazanfar, S., Humphreys, D.T., Murray, N.J., Tran, Y.T.H., et al. (2024). Integration mapping of cardiac fibroblast single-cell transcriptomes elucidates cellular principles of fibrosis in diverse pathologies. Sci. Adv. *10*, eadk8501. https://doi.org/10.1126/sciadv.adk8501.
12. Liu, X., Yin, K., Chen, L., Chen, W., Li, W., Zhang, T., Sun, Y., Yuan, M., Wang, H., Song, Y., et al. (2023). Lineage-specific regulatory changes in hypertrophic cardiomyopathy unraveled by single-nucleus RNA-seq and spatial transcriptomics. Cell Discov. *9*, 6. https://doi.org/10.1038/s41421-022-00490-3.
13. Guo, S.J., Gao, P.J., Wu, L.Y., and Zhu, D.L. (2009). Complement C3 is involved in adventitial fibroblast phenotypic differentiation induced by angiotensin-II and TGF-beta 1. Int. J. Cardiol. *137*, S74. https://doi.org/10.1016/j.ijcard.2009.09.248.
14. Andrianifahanana, M., Wilkes, M.C., Repellin, C.E., Edens, M., Kottom, T.J., Rahimi, R.A., and Leof, E.B. (2010). ERBB Receptor Activation Is Required for Profibrotic Responses to Transforming Growth Factor β. Cancer Res. *70*, 7421–7430. https://doi.org/10.1158/0008-5472.CAN-10-0232.
15. Helker, C.S., Eberlein, J., Wilhelm, K., Sugino, T., Malchow, J., Schuermann, A., Baumeister, S., Kwon, H.-B., Maischein, H.-M., Potente, M., et al. (2020). Apelin signaling drives vascular endothelial cells toward a pro-angiogenic state. Elife *9*, e55589. https://doi.org/10.7554/eLife.55589.
16. Daher, Z., Boulay, P.-L., Desjardins, F., Gratton, J.-P., and Claing, A. (2010). Vascular endothelial growth factor receptor-2 activates ADP-ribosylation factor 1 to promote endothelial nitric-oxide synthase activation and nitric oxide release from endothelial cells. J. Biol. Chem. *285*, 24591–24599. https://doi.org/10.1074/jbc.M110.115311.
17. Peng, Z., Zhang, R., Kuang, X., Yu, C., Niu, S., Du, Y., Lu, D., Li, S., Teng, Z., and Lu, S. (2022). Single-cell RNA-seq reveals interferon-induced guanylate-binding proteins are linked with sarcopenia. J. Cachexia Sarcopenia Muscle *13*, 2985–2998. https://doi.org/10.1002/jcsm.13091.
18. Yucel, N., Axsom, J., Yang, Y., Li, L., Rhoades, J.H., and Arany, Z. (2020). Cardiac endothelial cells maintain open chromatin and expression of cardiomyocyte myofibrillar genes. Elife *9*, e55730. https://doi.org/10.7554/eLife.55730.
19. Kawauchi, J., Zhang, C., Nobori, K., Hashimoto, Y., Adachi, M.T., Noda, A., Sunamori, M., and Kitajima, S. (2002). Transcriptional repressor activating transcription factor 3 protects human umbilical vein endothelial cells from tumor necrosis factor-alpha-induced apoptosis through down-regulation of p53 transcription. J. Biol. Chem. *277*, 39025–39034. https://doi.org/10.1074/jbc.M202974200.
20. Kalucka, J., de Rooij, L.P.M.H., Goveia, J., Rohlenova, K., Dumas, S.J., Meta, E., Conchinha, N.V., Taverna, F., Teuwen, L.-A., Veys, K., et al. (2020). Single-Cell Transcriptome Atlas of Murine Endothelial Cells. Cell *180*, 764–779.e20. https://doi.org/10.1016/j.cell.2020.01.015.
21. Schupp, J.C., Adams, T.S., Cosme, C., Raredon, M.S.B., Yuan, Y., Omote, N., Poli, S., Chioccioli, M., Rose, K.-A., Manning, E.P., et al. (2021). Integrated Single-Cell Atlas of Endothelial Cells of the Human Lung. Circulation *144*, 286–302. https://doi.org/10.1161/CIRCULATIONAHA.120.052318.
22. Rantakari, P., Auvinen, K., Jäppinen, N., Kapraali, M., Valtonen, J., Karikoski, M., Gerke, H., Iftakhar-E-Khuda, I., Keuschnigg, J., Umemoto, E.,

et al. (2015). The endothelial protein PLVAP in lymphatics controls the entry of lymphocytes and antigens into lymph nodes. Nat. Immunol. *16*, 386–396. https://doi.org/10.1038/ni.3101.

23. Horowitz, A., Yu, H., Pandey, S., Mishra, B., and Sahoo, D. (2024). C1QA is an invariant biomarker for tissue macrophages. Preprint at bioRxiv. https://doi.org/10.1101/2024.01.26.577475.
24. Fallas, J.L., Yi, W., Draghi, N.A., O'Rourke, H.M., and Denzin, L.K. (2007). Expression patterns of H2-O in mouse B cells and dendritic cells correlate with cell function. J. Immunol. *178*, 1488–1497. https://doi.org/10.4049/jimmunol.178.3.1488.
25. Stein, E.V., Miller, T.W., Ivins-O'Keefe, K., Kaur, S., and Roberts, D.D. (2016). Secreted Thrombospondin-1 Regulates Macrophage Interleukin-1β Production and Activation through CD47. Sci. Rep. *6*, 19684. https://doi.org/10.1038/srep19684.
26. Phipson, B., Sim, C.B., Porrello, E.R., Hewitt, A.W., Powell, J., and Oshlack, A. (2022). propeller: testing for differences in cell type proportions in single cell data. Bioinforma. Oxf. Engl. *38*, 4720–4726. https://doi.org/10.1093/bioinformatics/btac582.
27. Skinnider, M.A., Squair, J.W., Kathe, C., Anderson, M.A., Gautier, M., Matson, K.J.E., Milano, M., Hutson, T.H., Barraud, Q., Phillips, A.A., et al. (2021). Cell type prioritization in single-cell data. Nat. Biotechnol. *39*, 30–34. https://doi.org/10.1038/s41587-020-0605-1.
28. López-Otín, C., Blasco, M.A., Partridge, L., Serrano, M., and Kroemer, G. (2023). Hallmarks of aging: An expanding universe. Cell *186*, 243–278. https://doi.org/10.1016/j.cell.2022.11.001.
29. Aibar, S., González-Blas, C.B., Moerman, T., Huynh-Thu, V.A., Imrichova, H., Hulselmans, G., Rambow, F., Marine, J.-C., Geurts, P., Aerts, J., et al. (2017). SCENIC: single-cell regulatory network inference and clustering. Nat. Methods *14*, 1083–1086. https://doi.org/10.1038/nmeth.4463.
30. Dobner, S., Tóth, F., and de Rooij, L.P.M.H. (2024). A high-resolution view of the heterogeneous aging endothelium. Angiogenesis *27*, 129–145. https://doi.org/10.1007/s10456-023-09904-6.
31. Lago, J.C., and Puzzi, M.B. (2019). The effect of aging in primary human dermal fibroblasts. PLoS One *14*, e0219165. https://doi.org/10.1371/journal.pone.0219165.
32. Vidal, R., Wagner, J.U.G., Braeuning, C., Fischer, C., Patrick, R., Tombor, L., Muhly-Reinholz, M., John, D., Kliem, M., Conrad, T., et al. (2019). Transcriptional heterogeneity of fibroblasts is a hallmark of the aging heart. JCI Insight *4*, e131092. https://doi.org/10.1172/jci.insight.131092.
33. López-Otín, C., Blasco, M.A., Partridge, L., Serrano, M., and Kroemer, G. (2013). The Hallmarks of Aging. Cell *153*, 1194–1217. https://doi.org/10.1016/j.cell.2013.05.039.
34. Nicin, L., Wagner, J.U.G., Luxán, G., and Dimmeler, S. (2022). Fibroblast-mediated intercellular crosstalk in the healthy and diseased heart. FEBS Lett. *596*, 638–654. https://doi.org/10.1002/1873-3468.14234.
35. Sucharov, C.C., Mariner, P., Long, C., Bristow, M., and Leinwand, L. (2003). Yin Yang 1 is increased in human heart failure and represses the activity of the human alpha-myosin heavy chain promoter. J. Biol. Chem. *278*, 31233–31239. https://doi.org/10.1074/jbc.M301917200.
36. Wang, X., Zhang, G., Dasgupta, S., Niewold, E.L., Li, C., Li, Q., Luo, X., Tan, L., Ferdous, A., Lorenzi, P.L., et al. (2022). ATF4 Protects the Heart From Failure by Antagonizing Oxidative Stress. Circ. Res. *131*, 91–105. https://doi.org/10.1161/CIRCRESAHA.122.321050.
37. Hao, Y., Hao, S., Andersen-Nissen, E., Mauck, W.M., Zheng, S., Butler, A., Lee, M.J., Wilk, A.J., Darby, C., Zager, M., et al. (2021). Integrated Analysis of Multimodal Single-Cell Data. Cell *184*, 3573–3587.e29. https://doi.org/10.1016/j.cell.2021.04.048.
38. Germain, P.L., Lun, A., Meixide, C.G., Macnair, W., and Robinson, M.D. (2022). Doublet Identification in Single-Cell Sequencing Data Using scDblFinder. f1000research *10*, 979. https://www.ncbi.nlm.nih.gov/pmc/articles/PMC9204188/.
39. McGinnis, C.S., Murrow, L.M., and Gartner, Z.J. (2019). DoubletFinder: Doublet Detection in Single-Cell RNA Sequencing Data Using Artificial Nearest Neighbors - ScienceDirect. Cell. Syst. *8*, 329–337. https://www.sciencedirect.com/science/article/pii/S2405471219300730.
40. Yu, G., Wang, L.-G., Han, Y., and He, Q.-Y. (2012). clusterProfiler: An R Package for Comparing Biological Themes Among Gene Clusters. OMICS A J. Integr. Biol. *16*, 284–287. https://doi.org/10.1089/omi.2011.0118.
41. Carlson, M., and Falcon, S. (2019). Org. Mm. Eg. Db: Genome Wide Annotation for Mouse. R Package Version *3*, 10–18129.
42. Chen, E.Y., Tan, C.M., Kou, Y., Duan, Q., Wang, Z., Meirelles, G.V., Clark, N.R., and Ma'ayan, A. (2013). Enrichr: Interactive and Collaborative HTML5 Gene List Enrichment Analysis Tool. BMC Bioinf. *14*, 128. https://doi.org/10.1186/1471-2105-14-128.
43. Cortal, A., Martignetti, L., Six, E., and Rausell, A. (2021). Gene Signature Extraction and Cell Identity Recognition at the Single-Cell Level with Cell-ID. Nat. Biotechnol. *39*, 1095–1102. https://doi.org/10.1038/s41587-021-00896-6.
44. Piñero, J., Bravo, À., Queralt-Rosinach, N., Gutiérrez-Sacristán, A., Deu-Pons, J., Centeno, E., García-García, J., Sanz, F., and Furlong, L.I. (2017). DisGeNET: A Comprehensive Platform Integrating Information on Human Disease-Associated Genes and Variants. Nucleic Acids Res. *45*, D833–D839. https://doi.org/10.1093/nar/gkw943.
45. Kassambara, A., and Mundt, F. (2020). Factoextra: Extract and Visualize the Results of Multivariate Data Analyses. R Package Version 1.0.7. https://CRAN.R-project.org/package=factoextra.
46. Gu, Z. (2022). Complex Heatmap Visualization. iMeta *1*, e43. https://doi.org/10.1002/imt2.43.
47. Jin, S., Guerrero-Juarez, C.F., Zhang, L., Chang, I., Ramos, R., Kuan, C.-H., Myung, P., Plikus, M.V., and Nie, Q. (2021). Inference and analysis of cell-cell communication using CellChat. Nat. Commun. *12*, 1088. https://doi.org/10.1038/s41467-021-21246-9.
48. Van de Sande, B., Flerin, C., Davie, K., De Waegeneer, M., Hulselmans, G., Aibar, S., Seurinck, R., Saelens, W., Cannoodt, R., Rouchon, Q., et al. (2020). A Scalable SCENIC Workflow for Single-Cell Gene Regulatory Network Analysis. Nat. Protoc. *15*, 2247–2276. https://doi.org/10.1038/s41596-020-0336-2.
49. Bates, D., Mächler, M., Bolker, B., and Walker, S. (2014). Fitting Linear Mixed-Effects Models Using Lme4. Preprint at arXiv. https://doi.org/10.48550/arXiv.1406.5823.
50. Stuart, T., Srivastava, A., Madad, S., Lareau, C.A., and Satija, R. (2021). Single-Cell Chromatin State Analysis with Signac. Nat. Methods *18*, 1333–1341. https://doi.org/10.1038/s41592-021-01282-5.
51. EnsDb.Mmusculus.V79 Available online: http://bioconductor.org/packages/EnsDb.Mmusculus.v79/.accessed on 13 September 2024)
52. Zhang, Y., Liu, T., Meyer, C.A., Eeckhoute, J., Johnson, D.S., Bernstein, B.E., Nusbaum, C., Myers, R.M., Brown, M., Li, W., and Liu, X.S. (2008). Model-Based Analysis of ChIP-Seq (MACS). Genome Biol. *9*, R137. https://doi.org/10.1186/gb-2008-9-9-r137.
53. Fornes, O., Castro-Mondragon, J.A., Khan, A., van der Lee, R., Zhang, X., Richmond, P.A., Modi, B.P., Correard, S., Gheorghe, M., Baranašić, D., et al. (2020). JASPAR 2020: Update of the Open-Access Database of Transcription Factor Binding Profiles. Nucleic Acids Res. *48*, D87–D92. https://doi.org/10.1093/nar/gkz1001.
54. Yu, G., Wang, L.-G., and He, Q.-Y. (2015). ChIPseeker: An R/Bioconductor Package for ChIP Peak Annotation, Comparison and Visualization. Bioinformatics *31*, 2382–2383. https://doi.org/10.1093/bioinformatics/btv145.
55. Schep, A.N., Wu, B., Buenrostro, J.D., and Greenleaf, W.J. (2017). chromVAR: Inferring Transcription-Factor-Associated Accessibility from Single-Cell Epigenomic Data. Nat. Methods *14*, 975–978. https://doi.org/10.1038/nmeth.4401.

56. Zheng, G.X.Y., Terry, J.M., Belgrader, P., Ryvkin, P., Bent, Z.W., Wilson, R., Ziraldo, S.B., Wheeler, T.D., McDermott, G.P., Zhu, J., et al. (2017). Massively Parallel Digital Transcriptional Profiling of Single Cells. Nat. Commun. *8*, 14049. https://doi.org/10.1038/ncomms14049.

57. Moerman, T., Aibar Santos, S., Bravo González-Blas, C., Simm, J., Moreau, Y., Aerts, J., and Aerts, S. (2019). GRNBoost2 and Arboreto: Efficient and Scalable Inference of Gene Regulatory Networks. Bioinformatics *35*, 2159–2161. Oxford Academic Available online: https://academic.oup.com/bioinformatics/article/35/12/2159/5184284

58. What Is Cell Ranger ATAC? -Software -Single Cell ATAC -Official 10x Genomics Support Available online: https://support.10xgenomics.com/single-cell-atac/software/pipelines/latest/what-is-cell-ranger-atac.accessed on 13 September 2024)

STAR★METHODS

KEY RESOURCES TABLE

REAGENT or RESOURCE	SOURCE	IDENTIFIER
Chemicals, peptides, and recombinant proteins		
7-Aminoactinomycin D	R&D Systems	7121
Collagenase, type II, powder	Worthington	LS004189
ACK lysis buffer	Thermo Fisher Scientific	A1049201
Critical commercial assays		
Pacific Blue™ Annexin V/SYTOX™ AADvanced™ Apoptosis Kit	Thermo Fisher Scientific	A35136
Single Cell 3′ Library and Gel Bead Kit v.2	10x Genomics	PN-120237
Chromium i7 Multiplex kit	10x Genomics	PN-120262
Chromium Single Cell ATAC v2.1.0	10x Genomics	1000175
Data and Code Availability		
scRNA seq for mice heart nonCMs in 3, 12 and 24 months	This paper	GEO: GSE277702
scATAC seq for mice heart nonCMs in 3, 12 and 24 months	This paper	GEO: GSE277702
Analysis Code	This paper	Zenodo: 14014681 (https://doi.org/10.5281/zenodo.14014681)
Experimental models: Organisms/strains		
Mus musculus, C57BL/6J strain	The Jackson Laboratory	
Software and algorithms		
Cell Ranger v7.2.0	10x Genomics	https://www.10xgenomics.com/support/software/cell-ranger/7.2
Seurat v 4.0.1	Hao*, Hao* et al.[37]	https://satijalab.org/seurat/
scDblFinder v 1.18.0	Germain et al.[38]	https://bioconductor.org/packages/release/bioc/html/scDblFinder.html
DoubletFinder v 2.0	McGinnis et al.[39]	https://github.com/chris-mcginnis-ucsf/DoubletFinder
clusterProfiler v 4.0.5	Yu et al.[40]	https://bioconductor.org/packages/release/bioc/html/clusterProfiler.html
org.Mm.e.g.,.db v 3.13.0	Carlson and Falcon.[41]	https://bioconductor.org/packages/release/data/annotation/html/org.Mm.eg.db.html
Enrichr	Chen et al.[42]	https://maayanlab.cloud/Enrichr/
CelliD v 1.12.0	Cortal et al.[43]	https://www.bioconductor.org/packages/release/bioc/html/CelliD.html
Augur v 1.0.3	Skinnider et al.[27]	https://github.com/neurorestore/Augur
DisGeNET	Piñero et al.[44]	https://www.disgenet.com/
Factoextra v1.0.7	Kassambara[45]	https://rpkgs.datanovia.com/factoextra/index.html
ComplexHeatmap v 3.19	Gu et al.[46]	https://bioconductor.org/packages/release/bioc/html/ComplexHeatmap.html
CellChat v 1.6.1	Suoqin Jin et al.[47]	https://github.com/sqjin/CellChat
SCENIC v 1.3.1	Aibar et al.[29]	https://github.com/aertslab/SCENIC
GRNBoost2	Sande et al.[48]	https://arboreto.readthedocs.io/en/latest/
RCisTarget v 1.10.0	Aibar et al.[29]	https://bioconductor.org/packages/release/bioc/html/RcisTarget.html
AUCell v 1.20.2	Aibar et al.[29]	https://www.bioconductor.org/packages/release/bioc/html/AUCell.html
lme4 v 1.1-35.5	Bates et al.[49]	https://cran.r-project.org/web/packages/lme4/index.html
Signac v 1.12.0	Stuart et al.[50]	https://stuartlab.org/signac/

(*Continued on next page*)

Continued

REAGENT or RESOURCE	SOURCE	IDENTIFIER
EnsDb.Mmusculus.v79	Johannes et al.[51]	https://www.bioconductor.org/packages/release/data/annotation/html/EnsDb.Mmusculus.v79.html
MACS2 v 2.2.9.1	Zhang et al.[52]	https://github.com/macs3-project/MACS/
JASPAR 2020	Fornes et al.[53]	https://jaspar.elixir.no/
ChIPseeker v 1.36.0	Yu et al.[54]	https://bioconductor.org/packages/release/bioc/html/ChIPseeker.html
chromVAR v 1.22.1	Schep et al.[55]	https://www.bioconductor.org/packages/release/bioc/html/chromVAR.html

EXPERIMENTAL MODEL AND STUDY PARTICIPANT DETAILS

Mouse model

Animal studies were approved by the Institutional Animal Care and Use Committee (IACUC) of the University of North Caroline at Chapel Hill and conform to the National Institutes of Health (NIH) Guidelines for the care and use of laboratory animals. Male mice (C57BL/6J strain) aged at 3 months, 12 months, and 24 months were used for the experiments.

Heart collection and nonmyocytes isolation

Male mouse hearts at 3 months of age, 12 months of age, and 24 months of age were collected for non-cardiomyocyte isolation. In accordance with UNC-Chapel Hill LARC guidelines, all animals were anesthetized with isoflurane (1%–2%) for scRNA-seq and scATAC-seq experiments. The heart was removed as quickly as possible to ensure that it remained as fresh as possible for Langendorff perfusion, where hearts were still beating and immediately used for perfusion to avoid vessel clogging, which could occur with CO2 euthanasia. Hearts were perfused with a Langendorff apparatus as described with minor modifications.[8] Briefly, retrograde perfusion was performed through an aortic cannulation, and continuous flow of 16–24 drops/min was maintained in a Langendorff apparatus. Both ventricles were digested with 1 mg/mL collagenase IaI for 10–15 min, and the ventricles were further mechanically dissociated by pipetting. Then, the cell suspension was collected and filtered through a 100μm cell strainer. CMs were removed by centrifugation at 50*g* (200 rpm) for 3 min, and nonCMs were enriched by centrifugation at 450*g* (2,000 rpm) for 5 min. The pelleted nonCMs were treated with 1 mL red blood cell lysis buffer (Gibco) at room temperature (RT) and washed twice with wash buffer (4% FBS/PBS).

Single live cells were FACS-sorted by 7-Amino Actinomycin D (7-AAD, R&D Systems), and Pacific Blue-conjugated Annexin V and SYTOX (Thermo) staining. Following sorting, cell concentration and viability of each sample were counted using automated cell counter (LUNA system, Logos biosytems) plus Acridine orange (AO)/propidium iodide (PI) dual nuclear staining. Cell concentration was adjusted to $1x10^6$ cells/ml for subsequent scRNA-seq via 10x Gemonics platform. Cells (50,000 per sample) for scATAC-seq were subjected to lysis for 3min and counted again with cell counter to determine the viability (lower than 5%) and concentration again.

Single-cell transcriptome library preparation and sequencing

Single live cells were loaded to 10x Genomics Chromium chip per factory recommendations. Reverse transcription and library preparation were conducted using Chromium Single Cell 3′ Library and Gel Bead Kit v.2 and Chromium i7 Multiplex kit. Sequencing was performed on Illumina NextSeq 500 with a high output kit.

Single-cell ATAC library preparation and sequencing

The single nuclei were processed for library preparation (Chromium Single Cell ATAC v1.0) following manufactural instructions from 10x Chromium. Sequencing was performed on Illumina NOVAseq-S1 platform.

METHOD DETAILS

Single-cell RNA-seq data analysis

Raw sequencing reads were processed with Cell Ranger[56] v7.2.0 pipeline. For each sample, the raw FASTQ files were aligned to the mouse reference genome (refdata-gex-mm10-2020-A) using the cellranger count pipeline with default parameters. This step generated gene expression matrices for each sample individually.

Quality control and preprocessing

Quality control was performed using Seurat (version 4.0.1).[37] Cells were filtered based on gene expression metrics to remove low-quality cells and potential doublets. Specifically, cells with fewer than 1,500 detected genes or more than 7,500 detected genes were excluded from further analysis. Cells with mitochondrial gene content greater than 10% were also filtered out, as high mitochondrial content can indicate stressed or dying cells. Gene expression data were log-normalized using the NormalizeData function with a

scale factor of 10,000. The data were then scaled and centered using the ScaleData function. Doublets were identified and removed using scDblFinder (version 1.18.0)[38] and DoubletFinder (version 2.0).[39] Cells with high doublet scores as determined by these methods were excluded. An overview of the scRNA preprocessing workflow, including the filtering criteria and steps taken to process the data, is summarized in Figure S1A. The characteristics of the scRNA-seq data after preprocessing are presented in Figure S1E.

Dimensionality reduction and clustering

After preprocessing, samples were merged without integration using Seurat's merge function, as there were no significant batch effects observed between samples collected at different time points (See Figure S1C). Highly variable features (genes) were identified using the FindVariableFeatures function with the 'vst' method, selecting the top 2,000 genes for downstream analyses. Principal component analysis (PCA) was performed using the RunPCA function on the scaled data. The top 20 principal components were selected based on the elbow plot and the percentage of variance explained for further analysis. Uniform Manifold Approximation and Projection (UMAP) was employed for visualization of the data in two-dimensional space using the RunUMAP function with the selected principal components.

Cell clustering was performed using Seurat's FindNeighbors and FindClusters functions. The FindNeighbors function was run using the top 20 principal components to construct a shared nearest neighbor (SNN) graph. Clustering was conducted with the FindClusters function using a resolution parameter of 0.8, resulting in 21 distinct clusters.

Differentially expressed gene (DEG) analysis

After preprocessing and clustering, differential expression analysis was performed to identify marker genes for each cluster using Seurat (version 4.0.1).[37] The FindAllMarkers function was employed with the following parameters: minimum fraction (min.pct) of 0.5, log fold change threshold (logfc.threshold) of 1, and using the non-parametric Wilcoxon rank-sum test. p-values were adjusted for multiple comparisons using the Bonferroni correction. Genes were considered significantly differentially expressed if they met the criteria of adjusted p-value <0.05 and absolute average log fold change (|avg_log2FC|) >1.

Gene ontology (GO) over-representation analysis

To gain insights into the biological functions of the marker genes, GO over-representation analysis was conducted using the clusterProfiler package (version 4.0.5).[40] For each cluster, the list of marker genes was converted to Entrez IDs using the bitr function from the org.Mm.e.g.,.db package (version 3.13.0).[41] The enrichGO function was used with default parameters and GO terms with adjusted p-values less than 0.05 were considered significantly enriched. Adjusted p-values were calculated using the Benjamini-Hochberg method to control the false discovery rate.

Cell type annotation and validation

Cell identities were assigned based on the expression of known marker genes. Marker genes for each cluster (listed in Table S1) were analyzed using Enrichr[42] and curated from relevant literature. Based on this analysis, 21 clusters were manually annotated as follows: Fibroblasts (Fib.1 to Fib.6), Endothelial Cells (Endo.1 to Endo.7), Macrophages (MC.1 to MC.3 and MC/B-cells), B Cells, T Cells, Smooth Muscle Cells, and Neutrophils. To validate the clustering results, we employed CelliD (version 1.12.0),[43] an unbiased cell identity recognition tool. CelliD calculates cell identities based on SingleR methodology and a built-in reference of mouse cell types. The results from CelliD were consistent with our manual annotations, confirming the accuracy of our clustering and cell type assignments.

Identification of cell types affected by aging perturbations

To identify cell types affected by aging, we employed Augur (version 1.0.3),[27] a computational method that prioritizes cell types based on their molecular response to a biological perturbation. In this study, we focused on aging as the perturbation, comparing cells from three different age groups: 3, 12, and 24 months. Augur quantifies the separability of cells from different time points within each cell type using machine learning classifiers. For each cell type, we applied the calculate_auc function with default parameters to generate an Area Under the Curve (AUC) score. This score reflects the classifier's ability to distinguish cells from different age groups, with an AUC score of 0.5 indicating random separability and 1.0 indicating perfect separability. To further investigate the differential changes between time points, we used a permutation-based test as described in the Augur paper.[27] This test was applied to compare the magnitude of changes in cell type separability between different aging periods (e.g., 3 months vs. 12 months and 12 months vs. 24 months). The permutation test generates a null distribution of AUC differences by randomly permuting the labels for the experimental time points and recalculating the AUC differences across permutations. We then compared the observed AUC differences to the null distribution to identify cell types with significant age-related changes in their transcriptomic profiles. In addition to the default analysis, we explored the effects of parameter tuning on our results. We adjusted the number of trees in the random forest classifier (from 100 to 500), varied the number of features to consider at each split (mtry from 2 to 5), and changed the minimum number of samples required to split a node (min_n, set to both 0 and 10). These parameter configurations were applied to evaluate whether the AUC scores and the rank of cell types changed. While these adjustments resulted in slight differences in AUC values, the overall rank and biological interpretation remained consistent, indicating that our conclusions about cell-type-specific aging responses were robust across parameter settings (See Figure S6).

Using this combined approach of default and parameter-tuned analyses, we not only quantified the impact of aging within each cell type but also confirmed the consistency of the results across different classifier settings. This enabled us to assess the robustness of our findings regarding the dynamics of aging across early and late stages.

Gene set enrichment and pathway analysis

Gene set enrichment analysis was performed using AUCell (version 1.20.2) to score pathway activity in individual cells. Based on the normalized expression matrix by Seurat, the AUCell_buildRankings function ranked gene expression for each cell, and the AUCell_calcAUC function calculated the area under the curve (AUC) values for predefined gene sets. Myocardial fibrosis, heart failure, inflammation gene sets were obtained from the DisGeNET[44] database. The senescence-associated secretory phenotype (SASP) gene sets were sourced from the SenMayo gene set.[2]

Hierarchical clustering analysis

We performed hierarchical clustering on the log-fold change matrix of the DEGs using the Ward.D2 method. Distances between genes were calculated using Euclidean distance, and the resulting dendrogram was used to identify distinct clusters of DEGs that exhibited similar expression patterns across aging. To determine the optimal number of clusters, we used the elbow method using the fviz_nbclust function in factoextra.[45] The elbow point was used to select the number of clusters (k). Gene expression heatmaps were generated using the ComplexHeatmap[46] package. The rows of the heatmap represent the DEGs, and columns correspond to the time points. Heatmaps were annotated with the number of genes in each cluster, and color gradients were used to indicate log2 fold changes. For each identified gene cluster, we performed Gene Ontology (GO) enrichment analysis using the enrichGO function from the clusterProfiler (version 4.0.5).[40] GO terms with an adjusted p-value <0.05 were considered significantly enriched, and the results were visualized in bar plots.

Cell–cell communication analysis

Cell–cell communication between cell types was assessed using CellChat (version 1.6.1),[47] which infers and analyzes intercellular communication networks based on known ligand-receptor interactions. The normalized expression data and cell type annotations were input into CellChat. Significant interactions were identified using default parameters, with interactions reaching $p \leq 0.05$ considered significant. The communication networks were visualized using the netVisual_circle function, displaying the number and strength of interactions between cell types.

Transcriptional regulatory network analysis

To analyze transcriptional regulatory networks during non-cardiomyocyte (non-CM) aging, we employed the SCENIC workflow (version 1.3.1).[29] SCENIC integrates single-cell gene expression data to infer regulons—transcription factors (TFs) and their target genes. First, the co-expression network was inferred using GRNBoost2,[57] identifying genes co-expressed with TFs and separating targets into positively and negatively correlated groups. Next, RCisTarget (version 1.10.0) performed *cis*-regulatory motif analysis using the cisTarget databases (mm10 refseq_r80 v9 database) to select significantly enriched motifs among the co-expression modules. The TF-gene modules and target gene predictions were integrated to construct regulons. AUCell (version 1.20.2)[29] was then used to score regulon activity in each cell by calculating the AUC based on gene expression rankings. Regulons with TFs showing significant changes in expression (log fold change) during aging were identified to depict the impact of aging on transcriptional regulatory networks.

To investigate changes in transcriptional regulatory networks during aging, we employed linear mixed models (LMMs) to identify transcription factors (TFs) with significant shifts in average activity. LMMs account for both fixed effects (aging) and random effects (variability within and between cell types), thus handling the hierarchical structure of the data. We used the lme4[49] package (version 1.1–35.5) to fit the LMMs. The activity scores of TF regulons, calculated by AUCell in the SCENIC workflow, served as the response variable. The models included age as a fixed effect and random intercepts for cell type and individual sample to account for cell-type-specific variability and inter-individual differences.

Single-cell ATAC-seq data analysis

Sequencing reads from scATAC-seq experiments were processed using Cell Ranger ATAC (version 2.1.0).[58] The cellranger-atac count pipeline was used with default parameters to align reads to the mouse reference genome (mm10, refdata-cellranger-arc-mm10-2020-A-2.0.0) and generate fragment files for each sample.

Quality control and preprocessing

Analyses were conducted using the Signac package (version 1.12.0).[50] Gene annotations were obtained from the EnsDb.Mmusculus.v79[51] database. Quality control metrics were calculated to filter out low-quality cells. Cells were retained if they met the following criteria: nucleosome signal <4, transcription start site (TSS) enrichment score >3, blacklist ratio <0.05, peak region fragments between 3,000 and 30,000 and percentage of reads in peaks $\geq$15%. An overview of the scATAC preprocessing workflow, including the filtering criteria and steps taken to process the data, is summarized in Figure S1B. After preprocessing, samples were merged without integration using Seurat's merge function, as there were no significant batch effects observed between samples collected

at different time points (See Figure S1D). The characteristics of the scATAC-seq data after preprocessing are presented in Figure S1F. Cells not meeting these criteria were excluded from further analysis to ensure data quality and reliability.

Dimensionality reduction and clustering

The preprocessed scATAC data were normalized using term frequency-inverse document frequency (TF-IDF) transformation. We identified top features (peaks) using the FindTopFeatures function with a minimum cutoff of 'q0', which selects all features with non-zero counts. Singular value decomposition (SVD) was performed on the top features to reduce the dimensionality of the dataset and compute latent semantic indexing (LSI) components using the RunSVD function. UMAP was employed for non-linear dimensionality reduction using the RunUMAP function on the significant components from SVD. Clustering was performed using the Louvain algorithm via the FindNeighbors and FindClusters functions with a resolution parameter of 1.2. This clustering approach mirrored the procedure used in the scRNA-seq analysis.

Cell type annotation via label transfer

Cell types in the scATAC-seq data were annotated by transferring labels from the scRNA-seq dataset using Seurat's FindTransferAnchors and TransferData functions. This method identifies correspondences between the two datasets based on shared features, enabling the recognition of the 21 cell clusters corresponding to major non-cardiomyocyte (non-CM) cell types. Our downstream analysis focused on major subpopulations of fibroblasts (FBs), endothelial cells (ECs), and macrophages (MCs).

Differential accessibility analysis

Peak calling was performed using MACS2 (version 2.2.9.1)[52] for clusters with more than 100 cells. Differentially accessible regions (DARs) among cell types and subtypes were identified using the FindMarkers function in Signac and Seurat, conducting a differential accessibility (DA) test with default parameters. Peaks were considered significantly differentially accessible if they had p-values <0.05 and log fold change >0. For cell types or subtypes with fewer than 2,000 DARs, peaks were ranked based on their p-values, and the top 2,000 most significant peaks were selected as representative DARs for further analysis.

Motif enrichment and variability analysis

Motif enrichment analysis was performed to identify overrepresented transcription factor binding motifs in the differentially accessible peaks. A hypergeometric test was used to assess the probability of observing each motif at the given frequency by chance. The JASPAR 2020 non-redundant vertebrate motif database[53] was utilized as a reference. We annotated the genomic locations of DARs using ChIPseeker (version 1.36.0),[54] categorizing them into genomic features such as promoters, introns, and exons. Motif variability among cells was inferred using chromVAR (version 1.22.1),[55] which calculates deviations in motif accessibility across cells. Differentially active motifs between cell types were identified, providing insights into the regulatory dynamics.

QUANTIFICATION AND STATISTICAL ANALYSIS

Statistical analysis

Statistical analyses were conducted using R software (version 4.3.1). Unless otherwise stated, values are expressed as mean ± standard error of the mean (SEM) from two biologically independent samples. For differential gene expression analysis, the non-parametric Wilcoxon rank-sum test was used as implemented in Seurat's FindAllMarkers function. p-values were adjusted using the Bonferroni correction for multiple testing. Genes with adjusted p-values <0.05 were considered statistically significant. In the cell–cell communication analysis, interactions with p-values $\leq$0.05 were deemed significant. For differential accessibility analysis in scATAC-seq data, peaks with p-values <0.05 and log fold change >0 were considered significantly differentially accessible. Statistical significance levels are denoted as follows, p-value <0.05: statistically significant (*), p-value <0.01: highly significant (**), p-value <0.001: strongly significant (***).